VIP Energy-Storage Materials Very Important Paper

International Edition: DOI: 10.1002/anie.201800479
German Edition: DOI: 10.1002/ange.201800479

Engineering Fast Ion Conduction and Selective Cation Channels for a High-Rate and High-Voltage Hybrid Aqueous Battery

Chunyi Liu, Xusheng Wang, Wenjun Deng, Chang Li, Jitao Chen, Mianqi Xue, Rui Li,* and Feng Pan*

Abstract: *The rechargeable aqueous metal-ion battery (RAMB) has attracted considerable attention due to its safety, low costs, and environmental friendliness. Yet the poor-performance electrode materials lead to a low feasibility of practical application. A hybrid aqueous battery (HAB) built from electrode materials with selective cation channels could increase the electrode applicability and thus enlarge the application of RAMB. Herein, we construct a high-voltage K–Na HAB based on $K_2FeFe(CN)_6$ cathode and carbon-coated $NaTi_2(PO_4)_3$ (NTP/C) anode. Due to the unique cation selectivity of both materials and ultrafast ion conduction of NTP/C, the hybrid battery delivers a high capacity of 160 mAh g^{-1} at a 0.5 C rate. Considerable capacity retention of 94.3 % is also obtained after 1000 cycles at even 60 C rate. Meanwhile, high energy density of 69.6 Wh kg^{-1} based on the total mass of active electrode materials is obtained, which is comparable and even superior to that of the lead acid, Ni/Cd, and Ni/MH batteries.*

Lithium-ion batteries (LIBs) have been widely studied and successfully applied in various aspects of our daily lives. However, insufficient lithium resource and short lifetime make it a great challenge for LIBs.[1] As a result, there is an increasing amount of research activities focused on other rechargeable batteries (such as Na^+, K^+, Mg^{2+}, Al^{3+}, Zn^{2+}) and supercapacitors (or hybrid supercapacitors) as alternative energy-storage devices.[2] On account of similar chemical properties, greater abundant reserves, and lower costs, the sodium-ion battery (SIB) and potassium-ion battery (PIB) have been perceived as wonderful alternatives for the LIB.[3]

On the other hand, considering its appealing features of safety, cost effectiveness, and environmental friendliness, the rechargeable aqueous metal-ion battery (RAMB) has garnered great interest in the last two decades.[4] However, due to the large radius of K^+ and Na^+, only few reported materials could offer appropriate tunnels to transport Na^+ or K^+ ions in aqueous systems, such as $NaTi_2(PO_4)_3$, $Na_{0.44}MnO_2$, $Na_2CoFe(CN)_6$, $K_{0.27}MnO_2$, $KCuFe(CN)_6$, and so forth.[5] The side reactions like H_2/O_2 evolution reactions, proton co-intercalation of the alkali metal ions, and dissolution of electrode materials in aqueous electrolyte also make it more challenging to design and synthesize available materials for aqueous SIB and PIB.[6] Besides these drawbacks, low output voltage of those aqueous single-ion batteries, most below 1.2 V,[7] generally results in a low energy density that cannot meet the request of practical application. In this respect, hybrid batteries with two electrode materials possessing cation selectivity could not only combine respective advantages of the materials, but also improve the rate performance and coulombic efficiency. Hence, building structural stable framework for the electrode materials with fast ion conduction and selective cation channels could enable high battery performances.

Herein, we employ structural stable and high-capacity iron hexacyanoferrate compound $K_2FeFe(CN)_6$ (K-FeHCF) as cathode materials and carbon-coated $NaTi_2(PO_4)_3$ (NTP/C) as anode material to fabricate a high-voltage K–Na hybrid aqueous battery (HAB). The fast ion conduction (the K^+ diffusion coefficient of K-FeHCF is ca. 1.7×10^{-13} cm^2 s^{-1}, and the Na^+ diffusion coefficient of NTP/C is ca. 3.0×10^{-11} cm^2 s^{-1})[8] and selective cation channels (which is priority selection towards K^+ of K-FeHCF and single-Na^+ selectivity of NTP/C) of both cathode and anode materials ensure ultrahigh performances of the fabricated HAB.

Structures and morphologies of the K-FeHCF nanocubes and NTP/C nanocomposites were assessed by X-ray diffraction (XRD), scanning electron microscopy (SEM), and transmission electron microscopy (TEM). The XRD pattern of K-FeHCF (Figure 1 a) is readily indexed to the face-centered cubic structure of Prussian blue. According to the elementary composition of K/Fe (from ICP-AES), C/N (from elemental analysis) and crystal water (from TGA) content, the formula of K-FeHCF is simulated to be $K_{1.92}Fe[Fe(CN)_6]_{0.97}\cdot2.3H_2O$. Figure 1 b and c separately displays the SEM and high-resolution TEM (HRTEM) images of K-FeHCF. Cubic particles with an average size of 50 nm are obtained, which profits from the acid environment provided

[*] C. Liu, W. Deng, C. Li, Prof. M. Xue, Prof. R. Li, Prof. F. Pan
School of Advanced Materials
Peking University Shenzhen Graduate School
Shenzhen 518055 (China)
E-mail: xuemq@iphy.ac.cn
lirui@pkusz.edu.cn

X. Wang
Technical Institute of Physics and Chemistry
Chinese Academy of Sciences
Beijing 100190 (China)

X. Wang, Prof. J. Chen
Beijing National Laboratory for Molecular Sciences
College of Chemistry and Molecular Engineering
Peking University, Beijing 100871 (China)

Prof. M. Xue
Institute of Physics, Chinese Academy of Sciences
Beijing 100190 (China)

Supporting information and the ORCID identification number(s) for the author(s) of this article can be found under: https://doi.org/10.1002/anie.201800479.

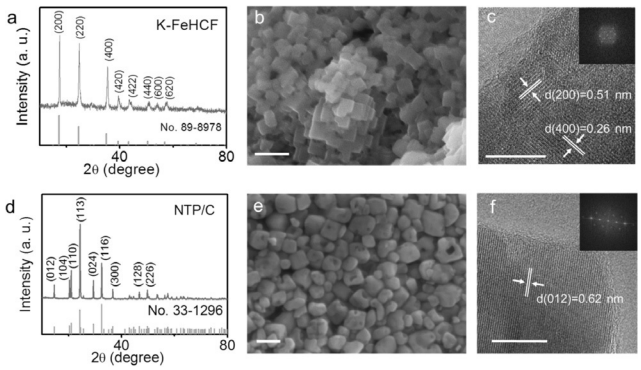

Figure 1. XRD (a,d) patterns, SEM (b,e) images, and HRTEM (c,f) images of the K-FeHCF and NTP/C, respectively. The scale bars in panels (b,c,e,f) are 200, 20, 200, and 10 nm, respectively. The insets of panels (c,f) are the corresponding Fast Fourier Transform (FFT) patterns.

by hydrochloric acid.[9] The (200) and (400) crystal planes are confirmed in Figure 1 c by the marked *d*-spacings of 0.51 and 0.26 nm, respectively. Figure 1 d shows the XRD pattern of NTP/C nanocomposite (with ca. 5 wt % carbon, see Figure S1 in the Supporting Information), indicating the pure phase of NTP/C.[10] The SEM image shown in Figure 1 e indicates an open holey structure of the NTP/C nanocubes with an average hole size below 50 nm, which could provide a faster Na^+ transport behavior and thus improve the electrochemical performances.[11] The HRTEM image shown in Figure 1 f illustrates a uniformly coated carbon layer, which is profitable to improve the electronic conductivity.[12]

The electrochemical behavior of K-FeHCF and NTP/C in either single-ion or mixed-ion electrolytes were investigated by cyclic voltammetry (CV) and galvanostatic voltage curves using a three-electrode system with a saturated calomel electrode (SCE) as reference electrode. Figure 2 a reveals CV curves of K-FeHCF tested in different aqueous electrolytes. The curve exhibits two pairs of well-separated and well-defined symmetric redox peaks at $+0.938/+0.871$ and $+0.304/+0.188$ V in electrolyte K. Such characteristic peaks are attributed to reversible valence changes between Fe^{II} and Fe^{III} during the K^+ storage/release processes on high-spin-state and low-spin-state sites, respectively. Herein, high-spin-state Fe sites are coordinated with nitrogen, while low-spin-state Fe sites are coordinated with carbon.[7] As for the case in electrolyte Na, a pair of splitting redox peaks at about 0 V is observed. This phenomenon results from the special feature of Na^+ during its insertion/extraction processes, since there are two different sites for the Na^+ ion due to the smaller volume compared to that of K^+. However, when there is K^+ neighboring, the extra site for Na^+ would be forbidden, therefore a split of redox peaks disappears in the mixed-ion electrolyte.[13] The first-cycle galvanostatic voltage profiles of K-FeHCF are illustrated in Figure 2 b. There are two flat charge/discharge plateaus for both electrolyte K ($+0.87/+0.86$ and $+0.25/+0.21$ V) and mixed-ion electrolyte ($+0.90/+0.88$ and $+0.26/+0.18$ V), while only one plateau which is centered at around 0 V and slightly slanted could be discovered for electrolyte Na. This is consistent well with the CV results. The first-cycle discharge capacity can reach 125 mAh g^{-1}, which is comparable to other excellent aqueous battery systems with potassium iron (II) hexacyanoferrate cathodes,[14] when using electrolyte K + Na and the corresponding initial charge–discharge efficiency could reach up to 96.5 %. Besides the high initial discharge capacity, the remarkable rate performance (Figure 2 c) also makes it preferable for HABs. Capacity of 41.0 mAh g^{-1} at 60 C rate (with the capacity retention of 32.8 %) is obtained when using electrolyte K + Na. At all current densities, higher capacities could be obtained in the mixed-ion electrolyte than the single-ion ones. Such phenomenon may be derived from the synergistic effect of Na^+ by inserting into the extra sites of Prussian blue framework.

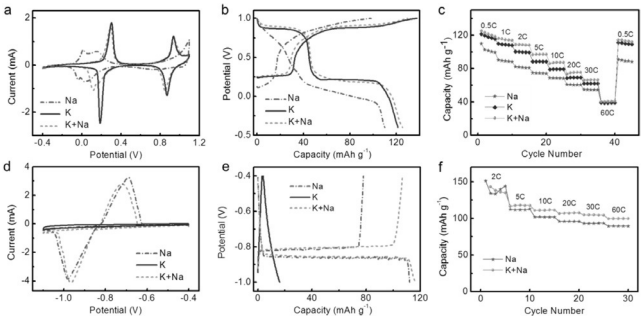

Figure 2. a) CV curves at a scan rate of 1 mV s^{-1} of K-FeHCF. b) First-cycle galvanostatic charge–discharge profiles of K-FeHCF versus SCE at 0.5 C rate. c) Rate performance of K-FeHCF. d) CV curves at a scan rate of 1 mV s^{-1} of NTP/C. e) Galvanostatic charge-discharge profiles of NTP/C versus SCE at 5 C rate. f) Rate performance of NTP/C. All above curves were tested in various electrolytes. The labeled K, Na, and K + Na represent aqueous electrolytes consisting of 0.5 M K_2SO_4, 0.5 M Na_2SO_4, and 0.25 M K_2SO_4/0.25 M Na_2SO_4, respectively.

Figure 2 d exhibits the CV curves of NTP/C in three-electrode system. There is one pair of redox peaks located at -0.994 and -0.649 V when measured in electrolyte Na, revealing the two-phase reaction mechanism while Na^+ migrates between electrode and electrolyte.[15] The mixed-ion electrolyte exerts a similar curve with a tiny shift of peaks, located at -0.968 and -0.713 V. This suggests that the existence of K^+ in the electrolyte would not influence the Na^+ insertion/extraction or that K^+ is unable to insert into the open-hole structural NTP/C nanocomposite for its larger ionic radius. The fact that no remarkable redox peaks appear in electrolyte K also bears witness to this conclusion. As the charge/discharge curves of NTP/C shown in Figure 2 e, a flat voltage plateau at -0.85 V and discharge capacity of 110 mAh g^{-1} are obtained in both electrolyte Na and mixed-ion electrolyte K + Na. However, there is no voltage plateau for electrolyte K and the specific capacity is only 16 mAh g^{-1}. Notable improvement of coulombic efficiency in mixed-ion electrolyte compared to single-ion electrolyte Na could also be clearly observed. Rate performance displayed in Figure 2 f suggests approximate capacity of NTP/C in electrolyte Na and K + Na. Since the capacity of NTP/C in electrolyte K is ignorable, it is not contained here.

To understand the ion-transport mechanism between the two electrode materials and mixed-ion electrolyte, the con-

tent of K and Na in K-FeHCF or NTP/C electrodes (normalized by Fe for K-FeHCF and Ti for NTP/C, respectively) before and after working were detected by using an energy dispersive X-ray spectroscopy (EDX). All electrodes were first fully cycled 100 times at 1 C, ending at full-discharge state. For K-FeHCF, larger total mole amount of K and Na in mixed-ion electrolyte K + Na than the other two electrolytes (Figure 3a) suggests that more ions may be

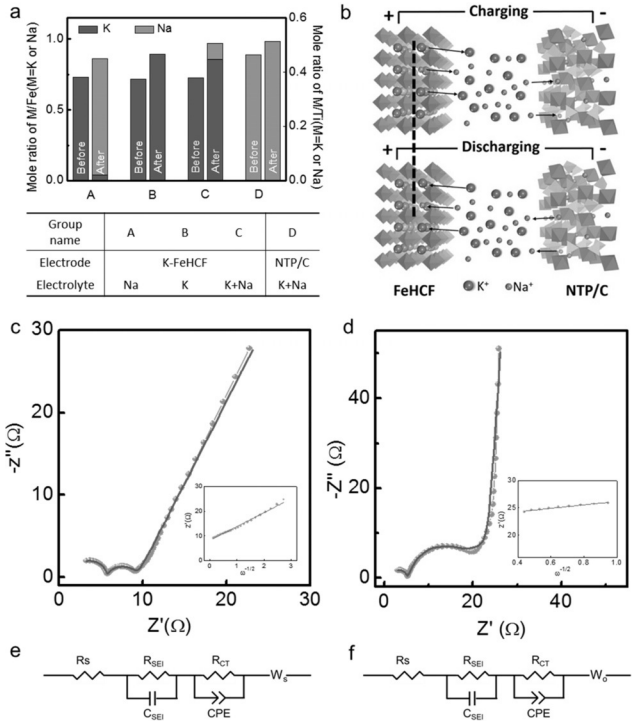

Figure 3. a) Element content of the K-FeHCF and NTP/C electrodes before and after 100 charge/discharge cycles at 1 C rate, respectively. b) Schematic of the K–Na HAB. EIS curves within the frequency range from 100 kHz to 10 mHz of the K-FeHCF in electrolyte K (c) and NTP/C in electrolyte Na (d), respectively. The insets are corresponding linear fitting curves. e,f) Equivalent electric circuits of the above EIS patterns.

introduced into the electrode materials during the charging process, and this may be the source of synergistic effect mentioned before. From the results of group using single-ion electrolyte Na, it could be concluded that Na^+ is able to insert into Prussian blue framework structure in kinetics. However, K^+ is still favorable for the mole ratio of Na/K is only 15.6% for mixed-ion electrolyte K + Na. This might have something to do with the lattice change of K-FeHCF nanocubes during the insertion/extraction of M^+ (M = K or Na).[5c,16] As for NTP/C, apparent single-selectivity of Na^+ is declared in Figure 3a. Based on the unique cation selectivity of both materials, an HAB based on open-framework K-FeHCF and NTP/C nanocomposite with open holey structure is assembled. Schematic diagram of the battery is demonstrated in Figure 3b. On the cathode side, the migration of two types of shuttle ions (Na^+/K^+) between the K-FeHCF electrode and electrolyte takes place, while there is only Na^+ migration on the anode side between the NTP/C electrode and electrolyte.

K^+ and Na^+ diffusion coefficients of the two electrode materials were calculated based on the results of electrochemical impedance spectroscopy (EIS) by the same three-electrode system. Figure 3c and 3d show the EIS curves of K-FeHCF and NTP/C, respectively. Their corresponding equivalent electric circuits are separately demonstrated in Figure 3e and 3f, in which R_{SEI} and R_{ct} severally represent the solid electrolyte interface resistance and charge-transfer resistance, and they conform to the two semicircles in high frequency region of both EIS curves. While Z_w represents the Warburg impedance, corresponding to the line part in low frequency region. Ion-diffusion coefficients of the two electrode materials could be calculated with following formula given in Equation (1),[17]

$$D = \frac{R^2T^2}{2A^2n^4F^4C^2\sigma^2} \quad (1)$$

where R is gas constant (8.314 $J K^{-1} mol^{-1}$), T is room temperature (298 K), A is the surface area of the electrode (3.85×10^{-5} m^2), F is the Faraday constant (96485 $C mol^{-1}$), C is the concentration of K^+ in K-FeHCF or Na^+ in NTP electrode, and σ is the slope of the line Z'-$\omega^{-1/2}$ (as shown in the insets of Figure 3c and d, the σ values are 5.67 and 3.16, respectively), n *is* the number of the electrons transferred in the electronic reaction. The insertion/extraction mechanisms of K-FeHCF and NTP/C can be described as following Equations (2) and (3),

$$K_2Fe^{II}[Fe^{II}(CN)_6] \cdot 2H_2O \leftrightarrow K^+ + KFe^{III}[Fe^{II}(CN)_6] \cdot 2H_2O + e^- \leftrightarrow 2K^+ + Fe^{III}[Fe^{III}(CN)_6] \cdot 2H_2O + 2e^- \quad (2)$$

$$NaTi_2(PO_4)_3 + 2Na^+ + 2e^- \leftrightarrow Na_3Ti_2(PO_4)_3 \quad (3)$$

which shows n is 2 for both electrodes. Hence, the calculated D_K of K-FeHCF is 1.7×10^{-13} $cm^2 s^{-1}$ and D_{Na} of NTP/C is 3.0×10^{-11} $cm^2 s^{-1}$. D_K is a relatively high level among all PIB electrodes and D_{Na} is higher than those of other SIB electrodes (10^{-11}–10^{-14} $cm^2 s^{-1}$),[8] which suggests fast K^+ conduction and ultrafast Na^+ conduction. Such fast ion conduction may account for improving electrochemical performances of the fabricated HABs, especially for higher capacity at high rate, better rate performance, and greater power density.[17a]

Figure 4a illustrates the galvanostatic voltage profiles of the HAB and individual anodes/cathodes versus SCE. The operating voltage ranges from 0.5 to 1.9 V, and the potentials of two discharging plateaus (at about 1.72 and 0.98 V) are higher than other known mixed-ion aqueous batteries (Table S1).[5c,6,7,16,18] Redox peaks of the CV curves in Figure 4b are consistent with the flat voltage, which are located at 1.82/1.65 and 1.14/0.95 V. The HAB system also demonstrates considerable discharge capacity of 160 $mAh g^{-1}$ at 0.5 C rate based on the mass of K-FeHCF. The rate capability is depicted in Figure 4c. The capacity retentions remain 86%, 79%, 71%, 63%, 51%, 44%, and 24% of those at 1, 2, 5, 10, 20, 30, and 60 C rates, respectively. The excellent capacity-recovery capability could also be found when the current rate

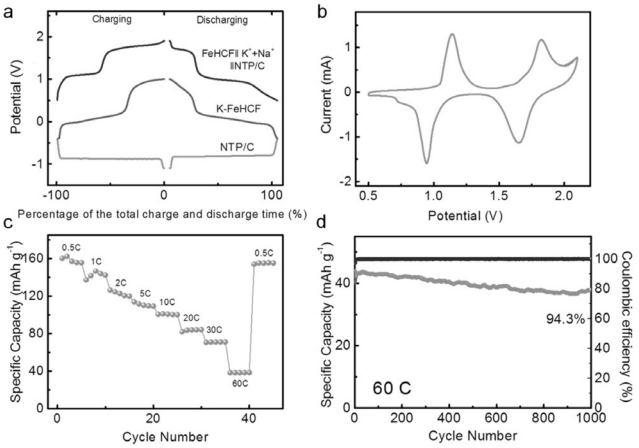

Figure 4. a) Galvanostatic profiles of the HAB along with the voltage profiles of their individual anode and cathode electrodes versus SCE at 1 C rate. b) CV curves of the HAB at a scan rate of 1 $mV s^{-1}$. c) Rate performance of the HAB. d) Long-term cycling stability of the HAB at 60 C rate.

returns back to 0.5 C rate with 96% retention of the initial capacity.

Excellent long-term cycling stability of this HAB is also manifested by high capacity retentions of 95.8% after 200 cycles at 5 C rate (Figure S2) and 94.3% after 1000 cycles at 60 C rate (Figure 4d) with stable coulombic efficiency at around 100%. The great reversibility can be attributed to the elimination of the side reaction. In addition, a specific energy of 69.6 $Wh kg^{-1}$ based on the total mass of active electrode materials is obtained at 0.5 C rate. The higher energy density of the mixed-ion battery compared with other Na^+ or K^+ aqueous batteries have been reported by Liu's groups.[7] The K-FeHCF//NTP/C HAB used in this work is not inferior with the previous ones in terms of energy density and average outputting voltage as shown in Figure 5, Figure S3 and Table S1.

In summary, a hybrid aqueous battery based on K-FeHCF and NTP/C with fast ion conduction and selective cation channels has been fabricated. It exhibits the highest specific capacity (160 $mAh g^{-1}$ based on the mass of cathode K-FeHCF) and energy density (69.6 $Wh kg^{-1}$ based on the total mass of active electrode materials) among the reported mixed-ion aqueous batteries based on alkalis-Li, Na, and K. Such high energy density is comparable and even superior to that of the lead acid, Ni/Cd, and Ni/MH batteries. Such battery system also reveals outstanding cycling stability at high rate. The investigation on the ion selectivity suggests that though K^+ is much more favorable than Na^+ when inserting into open-framework Prussian blue crystal, the existence of Na^+ could also contribute to improving the voltage and capacity. And NTP/C anode possesses strict selectivity on Na^+. The strategy to assemble hybrid battery by integrating two electrode materials with obvious or even strict cation selectivity towards different metal ions may provide guidance for enriching applicable electrodes of RAMBs.

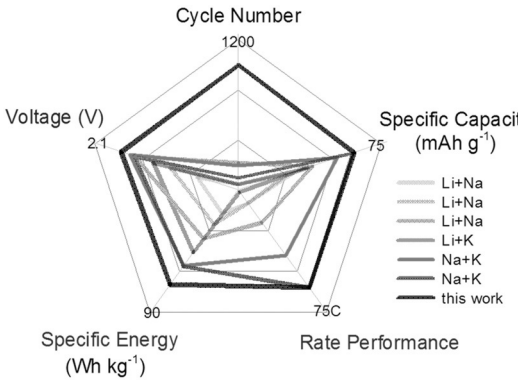

Figure 5. Performance comparison between the HAB designed in this work and other previous reported mixed-ion aqueous batteries.[5c, 6, 7, 16, 18]

Acknowledgements

This work was supported by the Shenzhen Science and Technology Research Grant (JCYJ20160531141109132, JCYJ20170412150450297), the National Natural Science Foundation of China (21622407, 21673008) and Guangdong Innovative and Entrepreneurial Research Team Progress (2013N080).

Conflict of interest

The authors declare no conflict of interest.

Keywords: batteries · energy-storage materials · fast ion conduction · ion selectivity · selective cation channels

How to cite: *Angew. Chem. Int. Ed.* **2018**, *57*, 7046–7050
Angew. Chem. **2018**, *130*, 7164–7168

[1] a) P. K. Nayak, L. Yang, W. Brehm, P. Adelhelm, *Angew. Chem. Int. Ed.* **2018**, *57*, 102–120; b) E. A. Olivetti, G. Ceder, G. G. Gaustad, X. Fu, *Joule* **2017**, *1*, 229–243; c) D. Chen, X. Wang, J. Chen, Z. Ren, M. Xue, G. Chen, *Adv. Mater.* **2015**, *27*, 4224–4228.

[2] a) L. Peng, Y. Zhu, D. Chen, R. S. Ruoff, G. Yu, *Adv. Energy Mater.* **2016**, *6*, 1600025; b) X. Wang, D. Chen, Z. Yang, X. Zhang, C. Wang, J. Chen, X. Zhang, M. Xue, *Adv. Mater.* **2016**, *28*, 8645–8650; c) X. Ma, M. Xue, F. Li, J. Chen, D. Chen, X. Wang, F. Pan, G. F. Chen, *Nanoscale* **2015**, *7*, 8715–8719; d) B. Li, F. Dai, Q. Xiao, L. Yang, J. Shen, C. Zhang, M. Cai, *Energy Environ. Sci.* **2016**, *9*, 102–106; e) M. Xue, D. Chen, X. Wang, J. Chen, G. F. Chen, *J. Mater. Chem. A* **2015**, *3*, 7715–7718.

[3] a) X. Wang, Z. Yang, C. Wang, L. Ma, C. Zhao, J. Chen, X. Zhang, M. Xue, *Nanoscale* **2018**, *10*, 800–806; b) Z. Jian, Z. Xing, C. Bommier, Z. Li, X. Ji, *Adv. Energy Mater.* **2016**, *6*, 1501874; c) X. Wang, Z. Yang, C. Wang, D. Chen, R. Li, X. Zhang, J. Chen, M. Xue, *J. Power Sources* **2017**, *369*, 138–145.

[4] H. Kim, J. Hong, K.-Y. Park, H. Kim, S.-W. Kim, K. Kang, *Chem. Rev.* **2014**, *114*, 11788–11827.

[5] a) Z. Li, D. Young, K. Xiang, W. C. Carter, Y.-M. Chiang, *Adv. Energy Mater.* **2013**, *3*, 290–294; b) X. Wu, M. Sun, S. Guo, J. Qian, Y. Liu, Y. Cao, X. Ai, H. Yang, *ChemNanoMat* **2015**, *1*, 188–193; c) Y. Liu, Y. Qiao, W. Zhang, H. Xu, Z. Li, Y. Shen, L. Yuan, X. Hu, X. Dai, Y. Huang, *Nano Energy* **2014**, *5*, 97–104;

d) M. Pasta, C. D. Wessells, N. Liu, J. Nelson, M. T. McDowell, R. A. Huggins, M. F. Toney, Y. Cui, *Nat. Commun.* **2014**, *5*, 3007.
[6] L. Chen, Q. Gu, X. Zhou, S. Lee, Y. Xia, Z. Liu, *Sci. Rep.* **2013**, *3*, 1946.
[7] L. Chen, H. Shao, X. Zhou, G. Liu, J. Jiang, Z. Liu, *Nat. Commun.* **2016**, *7*, 11982.
[8] a) C. Deng, S. Zhang, Y. Wu, *Nanoscale* **2015**, *7*, 487 – 491; b) X. Ren, Q. Zhao, W. D. McCulloch, Y. Wu, *Nano Res.* **2017**, *10*, 1313 – 1321.
[9] M. Hu, J.-S. Jiang, R.-P. Ji, Y. Zeng, *Crystengcomm* **2009**, *11*, 2257 – 2259.
[10] V. Aravindan, M. V. Reddy, S. Madhavi, S. G. Mhaisalkar, G. V. S. Rao, B. V. R. Chowdari, *J. Power Sources* **2011**, *196*, 8850 – 8854.
[11] L. Zhang, X. Wang, W. Deng, X. Zang, C. Liu, C. Li, J. Chen, M. Xue, R. Li, F. Pan, *Nanoscale* **2018**, *10*, 958 – 963.
[12] a) J. Wang, X. Sun, *Energy Environ. Sci.* **2012**, *5*, 5163 – 5185; b) M. Xue, Y. Wang, X. Wang, X. Huang, J. Ji, *Adv. Mater.* **2015**, *27*, 5923 – 5929.
[13] J.-Y. Liao, Q. Hu, B.-K. Zou, J.-X. Xiang, C.-H. Chen, *Electrochim. Acta* **2016**, *220*, 114 – 121.
[14] D. Su, A. McDonagh, S.-Z. Qiao, G. Wang, *Adv. Mater.* **2017**, *29*, 1604007.
[15] S. Patoux, C. Masquelier, *Chem. Mater.* **2002**, *14*, 5057 – 5068.
[16] P. Jiang, H. Shao, L. Chen, J. Feng, Z. Liu, *J. Mater. Chem. A* **2017**, *5*, 16740 – 16747.
[17] a) X. Wang, H. Hao, J. Liu, T. Huang, A. Yu, *Electrochim. Acta* **2011**, *56*, 4065 – 4069; b) Y. Xu, M. Zhou, X. Wang, C. Wang, L. Liang, F. Grote, M. Wu, Y. Mi, Y. Lei, *Angew. Chem. Int. Ed.* **2015**, *54*, 8768 – 8771; *Angew. Chem.* **2015**, *127*, 8892 – 8895.
[18] a) L. Chen, L. Zhang, X. Zhou, Z. Liu, *ChemSusChem* **2014**, *7*, 2295 – 2302; b) Y. Kong, J. Sun, L. Gai, X. Ma, J. Zhou, *Electrochim. Acta* **2017**, *255*, 220 – 229.

Manuscript received: January 18, 2018
Accepted manuscript online: March 14, 2018
Version of record online: April 17, 2018

